# Multicomponent broadband digital-based seismic landstreamer for near-surface applications

CrossMark

Bojan Brodic [a,*], Alireza Malehmir [a], Christopher Juhlin [a], Lars Dynesius [a], Mehrdad Bastani [b], Hans Palm [a]

[a] Department of Earth Sciences, Uppsala University, Villavägen 16, SE 75236, Uppsala, Sweden
[b] Geological Survey of Sweden, Villavägen 18, Box 670, SE 75128, Uppsala, Sweden

A B S T R A C T

During the last few decades there has been an increased demand for infrastructure, along with a greater awareness of environmental issues in the construction industry. These factors have contributed to an increased interest in using seismic methods for near surface characterization, particularly in urban environments. Seismic sensors not affected by anthropogenic electromagnetic noise are therefore important, as well as an acquisition system that is easy to deploy, move and non-invasive. To address some of these challenges, a multicomponent broadband MEMS (micro-electro mechanical system) based landstreamer system was developed. The landstreamer system is fully digital, therefore it is less sensitive to electrical or electromagnetic noise. Crosstalk, leakage and tilting tests show that the system is superior to its predecessors. The broadband nature of the sensors (theoretically 0–800 Hz), 3C (three-component) recording and the close spacing of the sensors enable high-resolution imaging. The current streamer configuration consists of 20 sensors 4 m apart and 80 sensors 2 m apart. The streamer can easily be combined with wireless recorders for simultaneous data acquisition. In this study, we present results from testing of the streamer with various sources, such as a shear wave vibrator and different types of impact sources. MEMS-sensors and their high sensitivity allowed recording clear reflections that were not observed with coil-based sensors. A complementary test was also carried out at a planned access ramp for an urban tunnel where potential poor quality rocks had been identified by drilling. First-break traveltime tomography showed that these poor quality rocks correlate with low velocity zones. The presented landstreamer system has great potential for characterizing the subsurface in noisy environments.

## 1. Introduction

Population growth with an increased demand for infrastructures, along with environmental considerations, motivate the need for better understanding of near surface geological conditions. In the last two decades, seismic method has became a common tool for shallow subsurface characterization, where new techniques and processing approaches have been developed (Bachrach and Nur, 1998; Bansal and Gaiser, 2012; Bretaudeau et al., 2008; Fabien-Ouellet and Fortier, 2014; Guy, 2004; Keho and Kelamis, 2009; Krawczyk et al., 2013; Malehmir et al., 2013a,b; Miller et al., 1986; Paasche et al., 2013; Polom et al., 2013; Pugin et al., 2004a,b, 2009, 2013a,b; Steeples and Miller, 1998; Steeples, 2004). Characterizing the shallow subsurface is particularly challenging in urban areas where anthropogenic noise, such as from power lines or traffic, among others, are present (Baker, 1999; Keho and Kelamis, 2009; Krawczyk et al., 2012; Polom et al., 2013; Pugin et al., 2004b; Steeples and Miller, 1998). In these environments, conventional planting of geophones is rarely possible and if several kilometers of seismic lines are to be acquired, with a limited number of channels, the whole spread has to be moved many times. Therefore, it is advantageous if the acquisition system is portable and geared for such conditions. To cope with all these issues, Uppsala University has developed a prototype 3C MEMS-based seismic landstreamer.

We can define a landstreamer as an array of sensors that can be pulled along the surface without the need for planting (Inazaki, 1999; Kruppenbach and Bedenbender, 1975; Suarez and Stewart, 2007). Eiken et al. (1989) applied the concept of towing a receiver array over land in the form of a snowstreamer and their work summarizes the preceding studies. The idea itself originates from the marine seismic industry and following the snowstreamer design, many authors have reported the usage of a towed land cable in various places and environments (Almholt et al., 2013; Determann et al., 1988; Huggins, 2004; Inazaki, 1999, 2004, 2006; Krawczyk et al., 2012; Link et al., 2006; Polom et al., 2013; Pugin et al., 2004a,b, 2009, 2013a,b; Pullan et al., 2008; Suarez and Stewart, 2007, 2008a; van der Veen et al., 2000, 2001; van der Veen and Green, 1998). Most of the reported studies

* Corresponding author at: Uppsala University, Villavägen 16, office EK221, SE 75236, Uppsala, Sweden.
*E-mail addresses:* bojan.brodic@geo.uu.se (B. Brodic), alireza.malehmir@geo.uu.se (A. Malehmir), christopher.juhlin@geo.uu.se (C. Juhlin), lars.dynesius@geo.uu.se (L. Dynesius), mehrdad.bastani@sgu.se (M. Bastani), hans.palm@geo.uu.se (H. Palm).

have been conducted with data acquisition systems that use different types of geophones, typically coil-based (Huggins, 2004). Although coil-based sensors dominate the market nowadays, numerous disadvantages have been noted during the half a century of their usage, among which one can mention electromagnetic (EM) noise pickup, limited bandwidth and sensitivity to tilting, especially for high-resolution and multicomponent imaging (Bansal and Gaiser, 2012; Deidda and Ranieri, 2001; Inazaki, 2004; Malehmir et al., 2013b; Pugin et al., 2004b). The bandwidth limitation is also becoming a more prominent issue in the field of full waveform inversion, where low frequencies are of interest (Adamczyk et al., 2014; Sirgue et al., 2010; Zhang et al., 2013). The same applies to surface-wave analysis of active seismic data (Fabien-Ouellet and Fortier, 2014; Lai et al., 2002; Park et al., 2002, 1999; Socco et al., 2009, 2010; Socco and Garofalo, 2012; Socco and Strobbia, 2004; Xia et al., 2003). In general, using geophone-type sensors, one either sacrifices low frequencies for obtaining high-resolution images of the subsurface or employs low-frequency geophones for surface-wave and/or full-waveform inversions. Aforesaid limitations, along with others (see Kendall, 2006; Mougenot and Thorburn, 2004), motivated the MEMS-based seismic landstreamer developed in this study. This is, to best of our knowledge, the first time that such a state-of-the-art landstreamer is presented and its reliability and potentials are illustrated.

We have assembled our landstreamer and tested it in various environments. Here we report results from two tests in our department's backyard in Uppsala and one from Stockholm where a large underground bypass tunnel is planned to be constructed within the next few years. Other studies with the system have also been carried out (and several others currently on-going; e.g. Malehmir et al., 2015). The recording abilities of the system have been tested using explosives as a seismic source, different size impact sources and a shear wave vibrator. In this paper, our main goal is to present separate studies conducted to validate the capability and reliability of the system for near surface applications. These include:

- comparison of the signals recorded with the landstreamer mounted MEMS-based sensors versus two planted lines with geophones of different resonance frequencies to check for potential unwanted issues of the streamer assembly and its signal quality;
- combination of wireless recorders with the streamer system to obtain information in areas where towing the streamer, or even planting geophones, was impossible;
- analysis of the frequency characteristics and shot gathers of the streamer recorded signal using a mini S-wave vibrator with different sweep ranges for near surface applications.

## 2. Fully digital multicomponent landstreamer

As a part of an academia-industry partnership project, a 3C MEMS-based seismic landstreamer was developed. The essential difference between the existing landstreamers (e.g., Huggins, 2004) and the one we present here is the digital nature of the sensors, implying fully digital data transmission. It is also much lighter and does not require several cables to power the line and transmit the data to an acquisition system. MEMS sensors measure ground motion as acceleration using a silicon chip with an approximate length of 1 cm, where the residual displacement between the inertial mass and the frame within the chip is on the order of a few nanometers (Gibson et al., 2005; Hons, 2008; Laine and Mougenot, 2014). One of the key benefits of the MEMS sensors is in their broadband linear amplitude and phase response, which allows recording frequencies from 0 to 800 Hz without attenuation (Hauer et al., 2008; Hons et al., 2007; Lawton et al., 2006a; Mougenot et al., 2011; Mougenot and Thorburn, 2004; Stotter and Angerer, 2011). Their resonant frequency (1 kHz) enables recording direct current related to gravity acceleration by which the gravity vector can be used for

sensitivity calibration and tilt measurements (Gibson et al., 2005; Kendall, 2006; Mougenot and Thorburn, 2004). A fundamental difference between MEMS sensors and geophones is in their performances. MEMS are designed to work below their resonance frequencies (e.g., below 1000 Hz) while geophones are designed to work above their resonance frequencies (e.g., generally above 4.5–40 Hz). Detailed studies have been conducted in the last decade comparing MEMS with different types of geophones and summarizing their pros and cons (e.g., Alcudia et al., 2008; Hauer et al., 2008; Hons et al., 2007; Hons, 2008; Laine and Mougenot, 2014; Lawton et al., 2006a; Mougenot et al., 2011; Stotter and Angerer, 2011; Suarez and Stewart, 2007, 2008a,b).

We aimed for a relatively light and portable data acquisition system that can be easily deployed, towed by any 2WD or 4WD (2 or 4 wheel drive) vehicle, combined with wireless units that are GPS time stamped (nanosecond accuracy), and used for a variety of applications and field situations. A great amount of time was spent to engineer the base plates "sleds" and materials holding the sensors (Fig. 1a, b). The sensors have been mounted on a non-stretchable belt used in the aircraft industry as cargo straps (Fig. 1b). The sleds weigh approximately 5 kg and with the sensors mounted on them provide excellent gravity based ground coupling (Fig. 1b). To avoid purchasing several telemetric data acquisition units (typically supporting 24 channels or nowadays 48), a decision was made to make the landstreamer based on the Sercel Lite technology and Sercel DSU3 sensors (MEMS-based mounted on the landstreamer). It is important to note that Sercel DSU3 sensors have a noise floor of 40 ng/Hz$^{1/2}$, which is approximately four times higher compared to conventional geophones (Gibson and Burnett, 2005; Hons, 2008; Laine and Mougenot, 2014; Merchant, 2009). The system architecture and the possibility to use up to 1000 active channels along with the Sercel Lite software represent an up-to-date standard in the seismic recording industry. In addition, the system provides sophisticated recording capabilities, such as supporting both geophone-type and MEMS-based sensors (but also hydrophones). Even though DSU3 sensors and the selected recording system are fairly expensive, obtaining the same amount of active channels with commonly used geophone-type telemetric data acquisition systems would require quite a number of them (e.g., 12–15 to come up with the same configuration as the streamer developed in this study). This fact, along with the 3C digital nature of the sensors, and the variety of possible field applications, make our landstreamer relatively comparable in terms of cost with existing telemetric data acquisition systems. With GPS being used for time stamping and data sampling, the system enables both passive and active data acquisition and their combination as well.

The current configuration of the landstreamer (September 2015) consists of five segments of 20 sensors each. Every segment connects to the next by a small trolley carrying a line-powering unit as shown by the red arrow in Fig. 1c. Four segments are of 20 units with 2 m spacing each, and the fifth consists of 20 units 4 m apart. The spacing of the units can be easily reduced in necessity of ultra-high resolution imaging. If longer offsets (than the overall streamer length of 240 m) are required, to obtain deeper penetration depth or imaging steeply dipping structures, wireless recorders (connected to geophones or MEMS-based sensors) can be used in combination. Wireless recorders can also be used to cover areas difficult to access with the streamer (an example of this set up is shown later in the paper). Table 1 summarizes the main characteristics of the streamer and compares it with the most commonly available ones.

In normal field conditions, data acquisition starts after approximately 1 h upon arrival to the site, with a team of 3 to 4 persons for the setup. Data acquisition rates have so far been varying from 600 m to 1200 m/day seismic line, using source and receiver spacings of 2 to 4 m. The shooting usually begins at the end of the spread and advances towards the beginning (where the observer sits in the towing vehicle). After recording all shot locations, the whole spread is moved forward to the next position. The last segment (20 units,
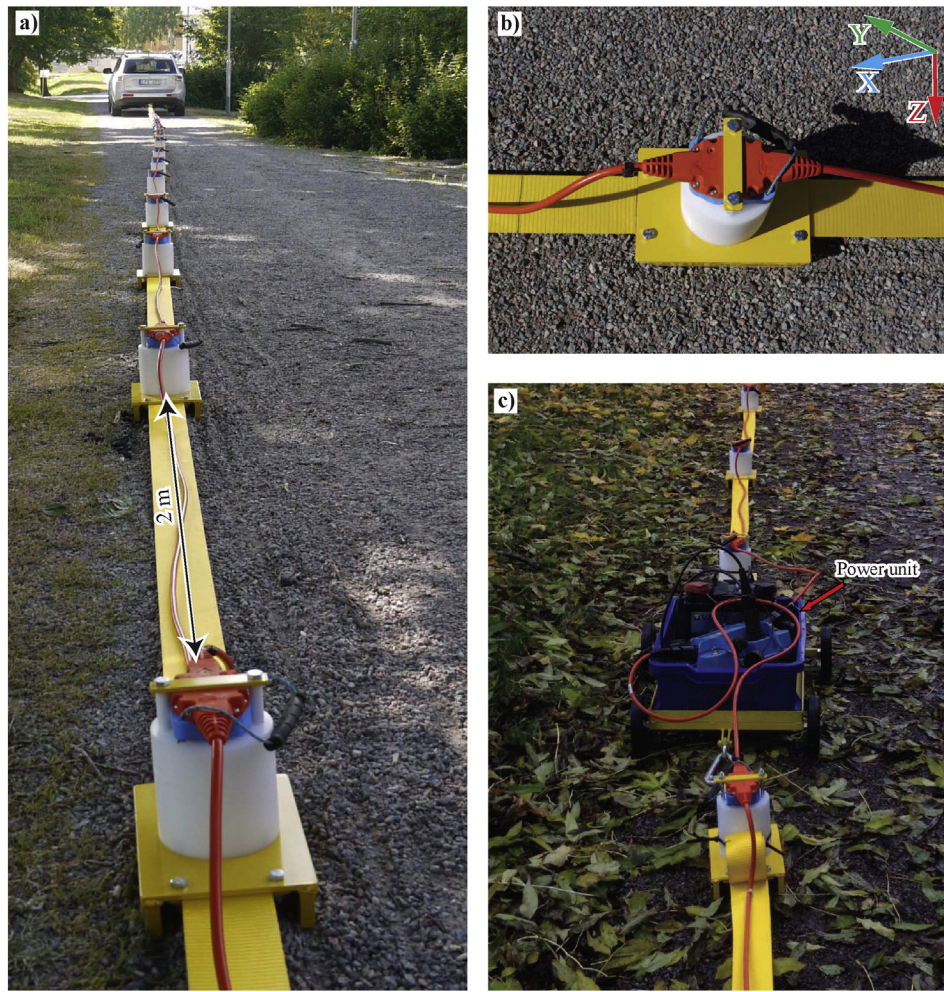
**Fig. 1.** (a) MEMS-based seismic landstreamer developed in this study towed by a relatively light vehicle. (b) A close-up showing the installation of the 3C sensor on the sled. (c) Small carriage connecting different segments (typically 20 sensors 2–4 m apart per segment) of the landstreamer carrying also a power unit. Photos were taken as a part of Backyard tests in Uppsala, Sweden at the early stage of the development of the streamer.

4 m spaced) often overlaps a portion of the previous landstreamer position allowing improved data coverage at the edge of each spread location and more favorable offsets if dipping structures are present.

## 3. Case studies

We have conducted several tests and contracted surveys since the streamer was actually assembled in June 2013, using different sources and in different weather conditions. This paper deals with three specific test studies that will be introduced and discussed. Tests I and II (referred

here as Backyard tests) were carried out in an open field in the early development stages of the streamer in the department's backyard at Uppsala University. The aim was to check the general reliability of the system. Test III was carried out in the northern outskirts of the city of Stockholm as a part of a major planned underground infrastructure project referred as the Stockholm Bypass (www.trafikverket.se/forbifartstockholm).

### 3.1. Backyard tests

The developed landstreamer benefits from constant improvements made by experiences from previous tests and surveys. Ease of access, well-known geology and almost no survey logistics in our department's backyard were ideal for checking different characteristics of the system at different development stages (Figs. 1, 2a). Geologically, this test site is located on an esker structure that consist of approximately 10–25 m of post-glacial sediments, typically fine-grained clays mixed with glacial tills, comprising the top most part of the esker. Deeper down there are coarse-grained materials overlaying granitic bedrock (Heijkenskjöld, 2001; Lundin, 1988).

#### 3.1.1. Test I — Reliability and advantages of the MEMS-based landstreamer
After assembling the first segment of the streamer of 20 DSU3 sensors spaced 2 m apart in July 2013, it was tested against two lines of 20 planted coil-based geophones (10 Hz and 28 Hz resonance

**Table 1**
Summary of the properties of the landstreamer system developed in this study.

| Parameters | Developed in this study | Existing landstreamers |
|---|---|---|
| Sensor type | 3C MEMS-based | Geophones (1C or 3C) |
| Frequency bandwidth | 0–800 Hz | 4.5–400 Hz |
| Tilt measurement | Recorded in the header | Not possible |
| Acquisition system | Sercel Lite (MEMS + geophones) | Most commonly Geometrics Geode (geophones only) |
| Max number of channels | 1000 | 24 (per unit) |
| Sensor spacing | Adjustable 0.2–4 m | Adjustable |
| Cabling | Single | Several |
| Data transmission | Digital | Analog |
| Data format | SEGD | SEG2 |
| GPS time | Recorded in the header | Often not possible |

**Fig. 2.** Photos showing details of the landstreamer versus planted geophones test. (a) Landstreamer was located in the middle of two planted geophone-type (10 Hz on the right-hand and 28 Hz on the left-hand side) lines. Note the difference in cabling involved for the planted lines and the streamer-mounted units. A sledgehammer was used as the seismic source in this study. (b) Side-by-side comparison between planted and streamer mounted 3C (DSU3, MEMS-based) sensors. This test was done to study different characteristics of the seismic wavefield registered on the streamer mounted sensors and if the sleds have some noticeable effects on the wavefield especially the horizontal components. A Bob-cat drop hammer was used as the seismic source in this study.

frequencies) with the same spacing. The aim was to compare the data quality recorded using DSU3s mounted on the landstreamer with the data recorded using the two planted geophone lines (Fig. 2a) and check for potential unwanted issues caused by the overall streamer assembly. The three lines were placed along a gravel bicycle-road; the same acquisition system was used enabling simultaneous recording of all the sensors for the three different line setups. First the assembled streamer segment was towed by a 4WD vehicle to a desired position; then aligned with the streamer sensors, vertical component geophones were planted on each side of the streamer (Fig. 2a; left side 28 Hz, 7 cm spike geophones, right side 10 Hz 7 cm spike geophones). We used a 5-kg sledgehammer as the seismic source. Shots were positioned at every streamer station and at each shot position we recorded 4 hits. These shot records were then vertically stacked to improve the signal to noise ratio. Shot gather quality of all three seismic lines was visually inspected, along with their amplitude spectra, especially for the vertical components. Due to unavailability, no planted horizontal component geophones were used, however, data recorded with the horizontal components of the DSU3s will be shown.

To enable a physically and mathematically correct data comparison, the geophone data need to be differentiated (or the DSU3 data integrated), implying that the comparison should be done in the same domain, either velocity or acceleration (Hons et al., 2007; Hons, 2008; Laine and Mougenot, 2014; Lawton et al., 2006a; Mougenot, 2014, personal communication). Since commercially available landstreamers are geophone based we choose to show the integrated DSU3 data, hence do the comparison in the velocity domain.

To complement the test, a separate study was conducted using 12-planted DSU3 sensors next to 12-streamer mounted DSU3 sensors on a site in south-west Finland (Fig. 2b). This was done to check for possible phase and time differences introduced by the sleds, especially for the horizontal components. Shots were fired along the whole landstreamer

length at a 4 m interval, while this set-up was in place. For these data a Bobcat-mounted drop hammer was used as seismic source (Place et al., 2015; Sopher et al., 2014). We present the data for trace-to-trace comparison between the planted and streamer sensors, after removing all the landstreamer sensors that had no accompanying planted pair. The approximately 50 m thick glacial and post-glacial sediments (confirmed by drilling; Jöni Mäkinen, 2014, personal communication) make this site favorable for this comparison since it is unlikely that any significant near surface geological effects will be present in the particle motions of the different phases.

*3.1.1.1. Results.* An example shot gather (after vertical stacking of the repeated shot records) presenting a comparison of the data from the two planted lines, with 10 and 28 Hz vertical geophones, and all three components (vertical and horizontal inline and crossline) of the landstreamer, with their corresponding amplitude spectra is shown in Fig. 3a, b, c, d, e. Fig. 3f, g shows an overlay of all the vertical component amplitude spectra with both DSU3 non-integrated and integrated data, scaled (Fig. 3f) and unscaled (Fig. 3g). All the amplitude spectra were calculated without using the three nearest-offset traces to minimize source noise contamination and the minor offset between the sensors on all three lines (the sensor pairs were located within 0.5 m radius). Some coherent features may be noted on almost all these data (shown by the red arrows), including the horizontal inline component of the DSU3 sensors. Horizontal component data have a time scale that is half that of the vertical component data to better compare the events marked by the red arrows. Based on the clearly observed reflection in the DSU3 vertical components (shown by the red arrow in Fig. 3c), it appears that the sensors mounted on the landstreamer recorded higher quality data compared with the geophones used here. Note that the reflection shown by the red arrow on Fig. 3a, c is not even observed on the 28 Hz geophones (Fig. 3b), which appears to be strongly contaminated
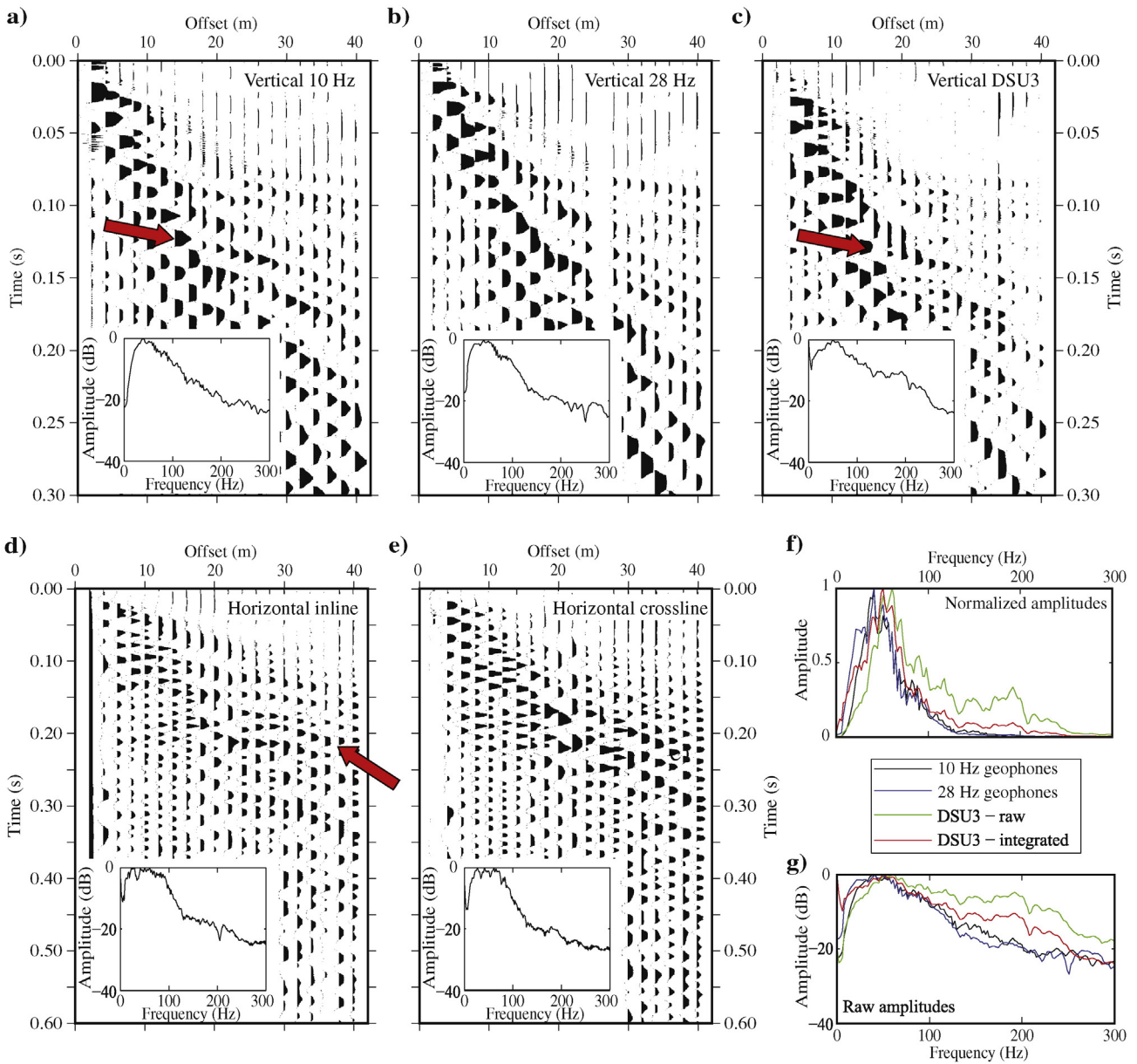
**Fig. 3.** An example shot gather (after vertical staking of three repeated shots) with the corresponding amplitude spectra from the first backyard test shown for (a) 10 Hz planted geophones, (b) 28 Hz planted geophones, (c) vertical component of the DSU3 sensors from the streamer, (d) horizontal inline component of the DSU3 sensors from the streamer and (e) horizontal crossline component of the DSU3 sensors from the streamer. (f) and (g) show amplitude spectra of all vertical components overlaid, normalized and raw, respectively, along with DSU3 vertical before and after integration. Note that MEMS data (acceleration) have been integrated to provide comparable data to the geophones (velocity) and the amplitude spectra calculated without three traces closest to the shot. AGC has been applied (100 ms window) for display purposes.

by surface waves. After integration, an amplitude increase of surface waves on the vertical component of the DSU3 sensors is generally observed (Hons et al., 2007; Hons, 2008, also notable from Fig. 3f, g), but in our case not as significant as to mask the reflection signal.

Fig. 4 shows an example shot gather from the side-by-side comparison of the planted and streamer mounted MEMS-based sensors (Fig. 2b). Here we also present particle motion plots (hodograms) of various wave types to judge if the sleds introduced suspicious particle motion. Particle motion plots from the noise part of the data (time window above the first arrivals) show slightly higher directionally dependent energy polarization on the horizontal crossline component while the other components have a more random character. This is likely due to wind and the wider nature of the frame holding the streamer sensor (acting as a barrier against wind; Fig. 1b) in this orientation. Otherwise, visual inspection of the particle motion plots does not

suggest any significant distortion introduced by the sled. Examination of the trace pairs of all components show identical phases with similar shape and arrival time, with a minor distortion on near offset traces of the horizontal crossline component that will be discussed later.

### 3.1.2. Test II — Micro shear wave vibrator test

To further explore the capabilities of the landstreamer, we also carried out a test using the micro shear wave vibrator — ELViS (Electro-dynamic Vibrator System; Krawczyk et al., 2012, 2013; Polom et al., 2011, 2013). The small size of the source, its easy handling, high signal reproducibility, no ground damage and low noise level make it attractive to be used with the streamer developed in this study, especially for urban applications. Example field photos from this test are shown in Fig. 5. ELViS version 3 (with a mounted horizontal shaker unit) enables generation of horizontally polarized (SH) seismic energy (see the green arrows in Fig. 5b),
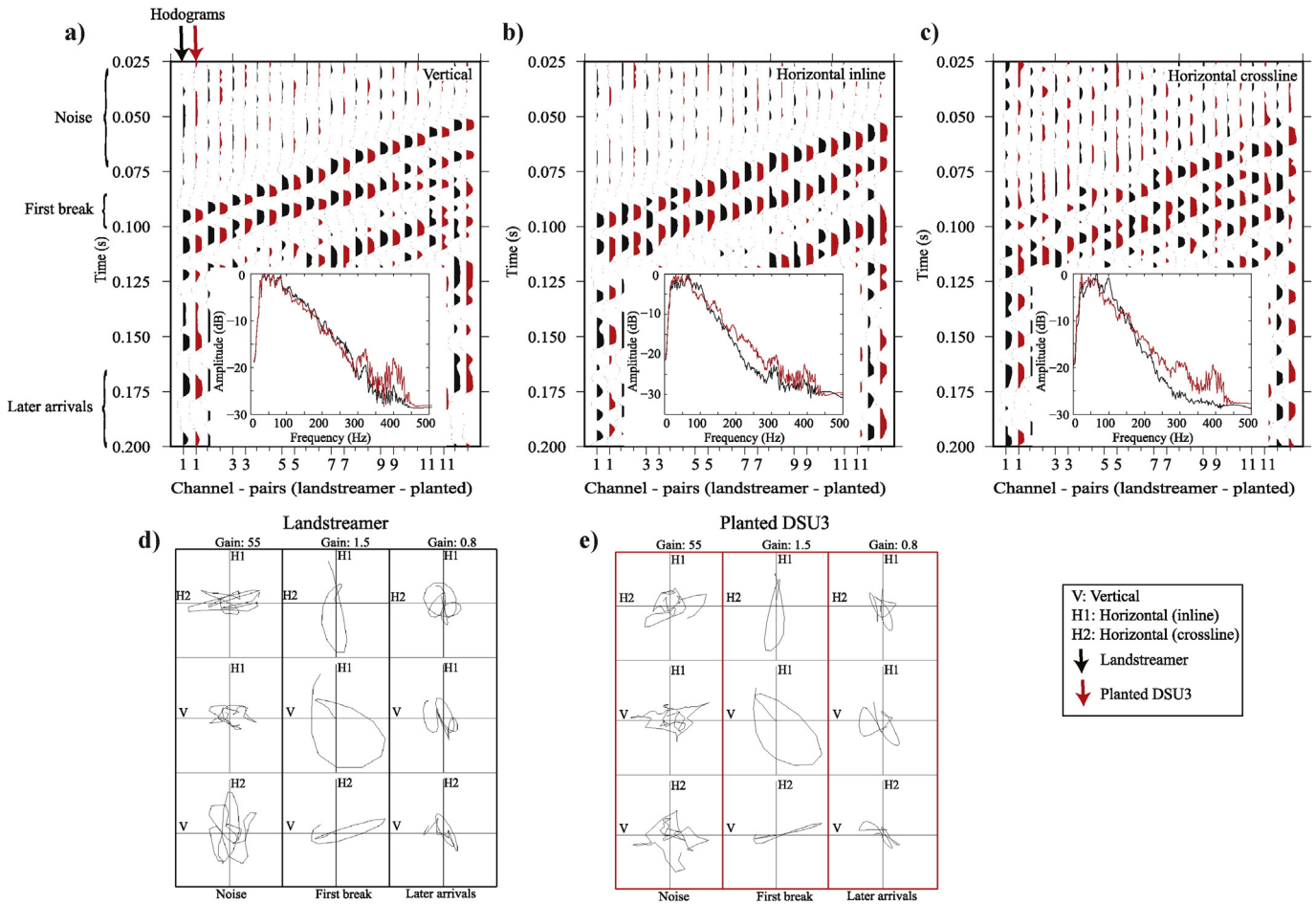
**Fig. 4.** An example shot gather (after vertical stacking of three repeated shots) from the side-by-side planted (black color wiggles) and streamer mounted (red color wiggles) DSU3 sensors test showing (a) vertical component data, (b) horizontal inline component data, (c) horizontal crossline component data. (d) Hodograms of noise, first break and later arrivals window from a far-offset trace from the streamer mounted sensor. (e) Hodograms of noise, first break and later arrivals time window of the same position trace but from the planted sensor. AGC has been applied (100 ms window) for display purposes. Data are shown in the acceleration (not integrated) domain given the identical nature of the sensors used in the test. Different gains were applied for the particle motion plots for display purposes.

implying that most of the energy should be recorded by the horizontal crossline component of our sensors. Signal control is carried out by a digital-to-analog sweep generator, which is fed by an EPROM (erasable programmable read-only memory) module, containing the desired sweep waveform (ELViS version 3 shaker is restricted to max 360 Hz). Car batteries, 12 V or 24 V, are used to power the source but also to increase the source-to-ground coupling because of their weight (Fig. 5b). In addition, often the source operator sits on it to further improve coupling as shown in Fig. 5a.

Typical shear wave surveys use an SH source and SH geophones (e.g., Bansal and Gaiser, 2012; Deidda and Ranieri, 2001; Garotta, 1999; Polom et al., 2013; Pugin et al., 2013a) to ease the processing (no need for complicated common conversion point binning or non-standard normal moveout corrections) and less contamination with other modes (Hardage et al., 2011). By changing the polarity of the first amplitude onset direction (positive or negative) and stacking two opposite polarity SH signals, minimization of vertical motion leaked into the SH component can be achieved (Garotta, 1999; Krawczyk et al., 2013; Polom et al., 2013).

During the shear wave source test, we acquired one line located perpendicular to the location of the line where the first backyard test was carried out, on a grassy field and with mainly postglacial clay-till sediments (Fig. 5a). We used only 2 segments of the landstreamer totaling 40 DSU3 units, spaced 2 m apart. ELViS with two sets of sweeps varying between 30 and 120 Hz and 30–240 Hz, and a 5-kg sledgehammer were used at every second station along the line. In the middle of the line,

shifted approximately 15 m in the perpendicular direction (Fig. 5a), a test using different sweep frequencies was conducted to check for signal attenuation on soft ground and the sensitivity of the streamer for weak shear wave signals coming off the line. The source sweep was 10 s long and recording time was 12 s long; a 1 ms sampling rate was used. At every vibrating point, we acquired 4 records, twice with both "positive" and "negative" polarities. Cross correlation was done using a pilot sensor registering the designed sweep. After cross correlation, source records (reduced to 2 s) were vertically stacked and used for studying signal penetration and amplitude spectra.

### 3.1.3. Results

The shear wave vibrator test (Fig. 5) was conducted without adjustment of the source frequencies to the ground conditions. Source sweeps were chosen randomly, which might have resulted in the lack of any clear reflections in the shot gathers. Fig. 6a shows an example shot gather with picked first breaks acquired using the 5-kg sledgehammer. Even though both selected sweeps (30–120 Hz and 30–240 Hz) appear not to be suitable and properly adjusted to the ground conditions, we were still able to pick the first breaks of shear waves, with a certain confidence, at least for the 30–120 Hz sweep (Fig. 6b). Fig. 6c shows a collocated shot gather acquired using the 30–240 Hz sweep, where higher noise levels can be seen and that the site attenuated higher source frequencies. First break picking here was extremely difficult and the data needed significant scaling. The collocated data recorded using the 30–120 Hz sweep served as a quality control set and allowed checking of
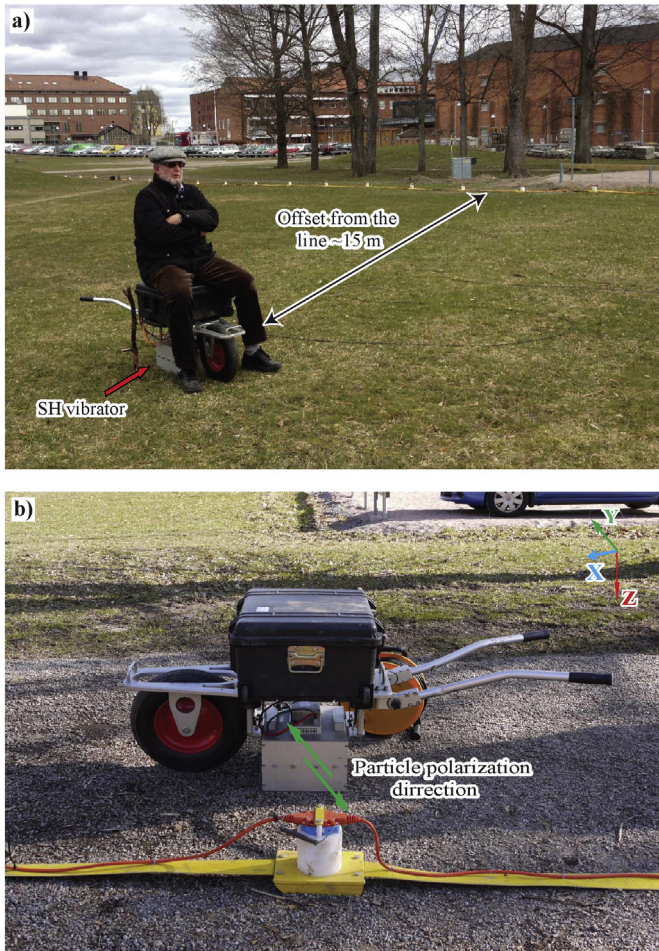
**Fig. 5.** Photos showing a micro shear wave vibrator (SH source) used in conjunction with the development of the streamer in another backyard test. (a) SH seismic source operating differing sweep frequency ranges but at about 15 m offset from the acquisition line. (b) A close up look at the SH-vibrator with the green arrows representing direction in which the energy is induced (SH–SH data acquisition).

the picked first breaks on the 30–240 Hz gathers. Fig. 6d shows the amplitude spectra of a different frequency range sweep test carried out along the line, with the source positioned with certain offsets from it (see Fig. 5a). Comparison between Fig. 6a and b, c suggests no significant P-wave energy leaked into the horizontal components after the cross-correlation and stacking of the opposite polarity records. It can also be observed from Fig. 6d that, at this site, no significant seismic energy can be seen above 100 Hz, regardless of the source sweep frequency used.

### 3.2. Test III — Stockholm Bypass

This survey was carried out in the framework of a nation-wide academia-industry joint project (Transparent Underground Structures; TRUST). Stockholm Bypass (also known as Förbifart Stockholm) is a planned underground highway (8 lanes) approximately 21 km long of which more than 17 km is to be tunnel through crystalline bedrock (www.trafikverket.se/forbifartstockholm). It will pass under 3 water bodies, with the deepest point reaching approximately 85 m below sea level. A test site where an access ramp for the tunneling will start, "Vinsta", located in the northern part of Stockholm city was chosen for the streamer test (Figs. 7, 8). Motivation to carry out the test at this site was a priori knowledge about a potential weak zone identified by a number of geotechnical boreholes suggesting poor rock quality (geotechnical Q-value below one) close to where the two seismic lines

were designed to intersect each other (Fig. 8). The geophysical objectives of the study were to evaluate the potential of the landstreamer in such a noisy environment, combination of the streamer with wireless units, obtaining information about depth to the bedrock and velocity information that may be linked to the rock quality, especially where the poor quality rocks were inferred to be present.

#### 3.2.1. Data acquisition

During November 2013, we acquired two seismic lines (Lines 1 and 2; Fig. 8) at the site. Due to the urban nature of the site, after a reconnaissance, a decision was made to conduct the whole survey at night to avoid heavy traffic and, most importantly, trams passing next to one of the seismic lines (Line 2). Although we managed to avoid "rush hours", there was still significant traffic during the whole survey time, including trams passing every few minutes up until midnight (Fig. 7b) and heavy trucks passing due to accessibility to the city during the night hours. The trams stopped for four hours during the nights for maintenance between 1 a.m. and 5 a.m., thus allowing a time slot to conduct the survey.

Geologically, both lines cross over areas with variable thickness glacial and post-glacial clays and tills ranging from 1 m to 20 m, overlaying a bedrock consisting of granites, granodiorites and monzonites (Olof Friberg, 2014, personal communication). Bedrock outcrops in several places, especially along Line 2, and their locations were noted during the data acquisition for direct comparison with results obtained in this work. North of Line 1, on the opposite side of the road and our line, rock outcrops were conspicuous, suggesting that the road (Fig. 8) is situated within a depression zone. On the LiDAR (Light Detection And Ranging) data (Fig. 8b), outcropping bedrock is evident where large topographic features are observed.

Line 1 had low topographic relief and was located parallel to the road and almost straight with no bedrock outcrops notable along the whole 560 m length. Data acquisition was done using three segments of the landstreamer (two segments with sensors 2 m apart and one with sensors 4 m apart, in total 160 m long). We used a 5-kg sledgehammer hitting a metallic plate at every 2 m to generate seismic energy. Shots were only activated along the two segments with 2 m station spacing; the remaining segment was used for obtaining data coverage in the zones between the streamer segments and providing far offset data. The spread was moved five times after first deployment. The data acquisition along Line 1 involved a team of five persons and took approximately 8 hours (during the night) to acquire.

Line 2 was logistically challenging due to many factors, such as vicinity to the tram tracks (Fig. 7b), severe topography (Fig. 7c), bedrock outcropping, a major road in the middle (Fig. 8) and concrete stairs for access to the tram station (Fig. 7a) where four sensors of the initial spread deployment had to be placed. It was acquired using a combination of the streamer with 3C wireless recorders of the same type (DSU3) as used in the streamer (Figs. 7, 8). The wireless recorders use a built-in GPS antenna for time stamping and data sampling. Six recorders on each side of the road continuously recorded data during the whole survey time and were kept at their positions while data acquisition continued from one to the other side of the road (see the black points in Fig. 8). After the survey, GPS time stamps of the active data from the landstreamer were used to extract the data from the wireless recorders. These data were later merged with the streamer data and treated similarly for further analysis and use. The information obtained from the wireless units was critical for delineating a zone of poor quality rock close to the road and slightly under it. Without the wireless recorders, it would have been difficult to achieve active signal recordings on both sides of the road using either the landstreamer or any other conventional cabled seismic data acquisition system. The three segments (120 m long) were used on the eastern side, but after moving to the western side of the road we decided to reduce the number of segments to two (in total 80 m long), due to inaccessibility and safety issues for bicycles passing the line overnight. Unfortunately, this reduction
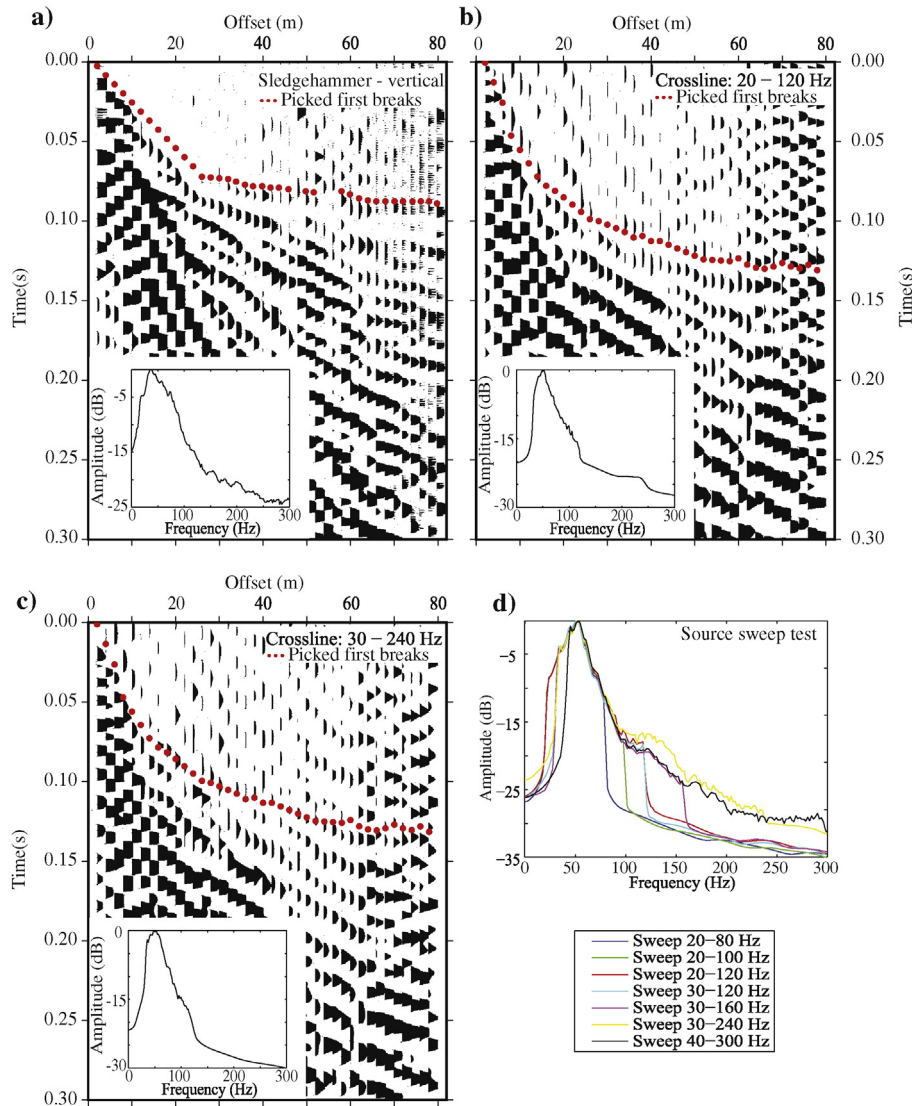
**Fig. 6.** Shot gathers and amplitude spectra for the data acquired in the second backyard test. (a) Shot gather showing vertical component data obtained using sledgehammer as a source. (b) Horizontal crossline component acquired with the ELViS micro shear vibrator and source sweep frequencies of 30–120 Hz. (c) Shot gather acquired with ELViS and source sweep frequencies 30–240 Hz. (d) Amplitude spectra showing different source sweep ranges test. Note that all the sweeps have almost the same dominant frequency and the signal rapidly attenuates after 100 Hz frequency. For all the shot gathers we used a fixed AGC (100 ms) for plotting purposes and no trace balancing or normalization was applied.

resulted in a lack of data coverage in some zones. The streamer was moved three times on the western side and was fixed on the eastern side, forming a line totally 420 m long (Fig. 8). All the sensor locations were accurately surveyed using a DGPS (differential GPS) system, with an elevation accuracy of a few centimeters, on both lines. Our standard procedure is to survey the coordinates of every streamer unit after deploying them. Each time the streamer is moved, the process is repeated. The wireless units record their coordinates from the GPS automatically, but for high-resolution seismic surveys with dense sensor spacing, the accuracy of this automatic positioning is judged to be inadequate. Hence, the wireless units get surveyed with the DGPS system as well.

*3.2.2. Shallow reflections and their imaging potentials*

Even in such a noisy environment, reasonably good quality first breaks were observed, especially after vertical staking of the repeated shot records. Example shot gathers from the two lines are shown in Fig. 9. Note the different quality data from these two lines. It is important to note that none of these shots acquired along the two lines show any evidence of spike frequencies (e.g., 50 Hz) from the tram

and high-voltage power-lines although they are just a few meters away. This is encouraging given one of the main aims of the streamer was to avoid recording this type of noise.

We spent a significant amount of time for reflection data imaging through various processing approaches. Some shots showed indications of reflections, but not enough convincing. Several stacked sections were generated, but at the end reflections in them believed to be highly contaminated by the remaining parts of source-generated noise, mainly direct and refracted P- and S-wave arrivals. Major problem here were both elevation and field statics. To further evaluate the reflection potential in the data, we carried out seismic elastic finite-difference modeling using a 1D model based on the direct and refracted arrival times for an estimate of the overburden thickness from the crossover distances (Fig. 9b, f). Two scenarios, $V_P/V_S = 5$ and $V_P/V_S = 2.5$, using a three layered earth model (5.5 m thick down to the water-table, $V_P = 500$ m/s, $V_S = 100$ m/s, $\rho = 1600$ kg/m$^3$; 7.5 m down to bedrock, $V_P = 2500$ m/s, $V_S = 500$ m/s, $\rho = 1900$ kg/m$^3$; and bedrock $V_P = 5800$ m/s, $V_S = 3400$ m/s and $\rho = 2750$ kg/m$^3$) were used for the modeling. The first scenario with $V_P/V_S = 5$ corresponds to our actual field situation, while the second one served as a test of the detection ability for more

**Fig. 7.** Photos showing field condition along Line 2 at the access ramp of Stockholm Bypass at the Vinsta site. (a) Landstreamer units placed at the staircase as a part of the first spread deployment along this line, spacing of 4 m streamer segment reduced to 2 m. (b) Combination of the landstreamer sensors with 12 MEMS-based wireless recorders to cover the inaccessible zone; at the major road cutting the line into two segments. (c) Tram passing during the data acquisition, location of the wireless units on both sides of the road and a view showing the severe topographic variations from one side of the line to another.

common field conditions. Synthetic shot gathers were generated using both elastic and acoustic media with a code available in Seismic Unix (Juhlin, 1995; Juhlin et al., 2012). A Ricker wavelet using a central frequency of 75 Hz, estimated by studying the amplitude spectra of the real data (Fig. 9a, b), was used to generate the synthetic seismograms. After detailed examination and comparison of the synthetic (Fig. 9c, d) and real field shot gathers (Fig. 9a, b), we concluded that the characteristics of the site, along with the source and acquisition set-up used, impairs the detection of the reflected energy from the bedrock in this survey. Reflected energy from the

bedrock (see the theoretical traveltimes shown in Fig. 9c, d) is interpreted to occur within the shear wave arrivals and unlikely to be observed after processing. The direct and refracted arrivals are quite consistent both in time and offset when comparing the synthetic and real shot gathers. This is an indication that the model used to generate the synthetic data is a reliable representation of the subsurface. During inspection of the shot gathers on Line 2, no prominent reflection was observed; most likely due to exposed bedrock and thin overburden, hence there was no need for generating synthetic data for this line.
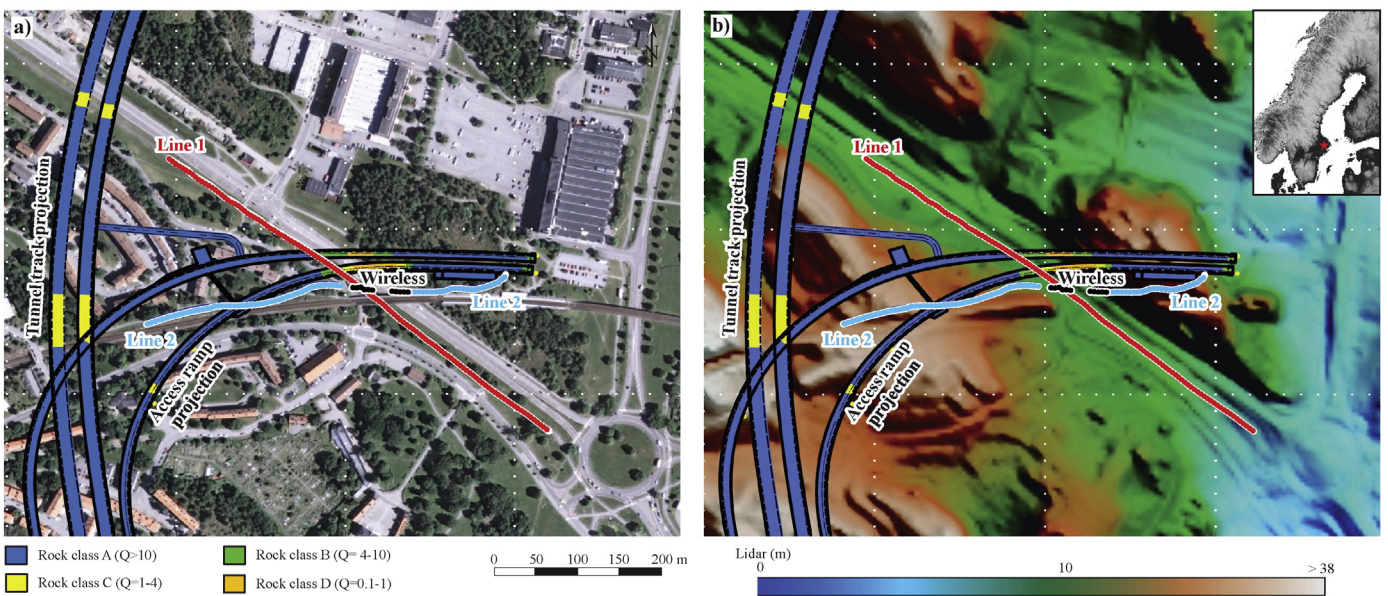


**Fig. 8.** Location of seismic lines (Lines 1 and 2) with respect to the planned access ramp and the main tunnel projected to the surface (a) aerial photo and (b) LiDAR (elevation) map. Colors on the tunnel track and access ramps show different rock classes identified from geotechnical boreholes. Twelve MEMS-based wireless recorders, six on each side of the road, are marked with the black points. Geotechnical data were kindly provided by the Swedish Transport Administration (Trafikverket).

### 3.2.3. Tomography, borehole data and 3D visualization

Since our targets were depth to the bedrock and the poor quality rocks inferred from the drilling at the site (Fig. 8a), we performed P-wave first break tomography using the PS_tomo 3D diving-wave tomography code (Tryggvason et al., 2002; Tryggvason and Bergman, 2006). The tomography was done in 3D to fully account for the
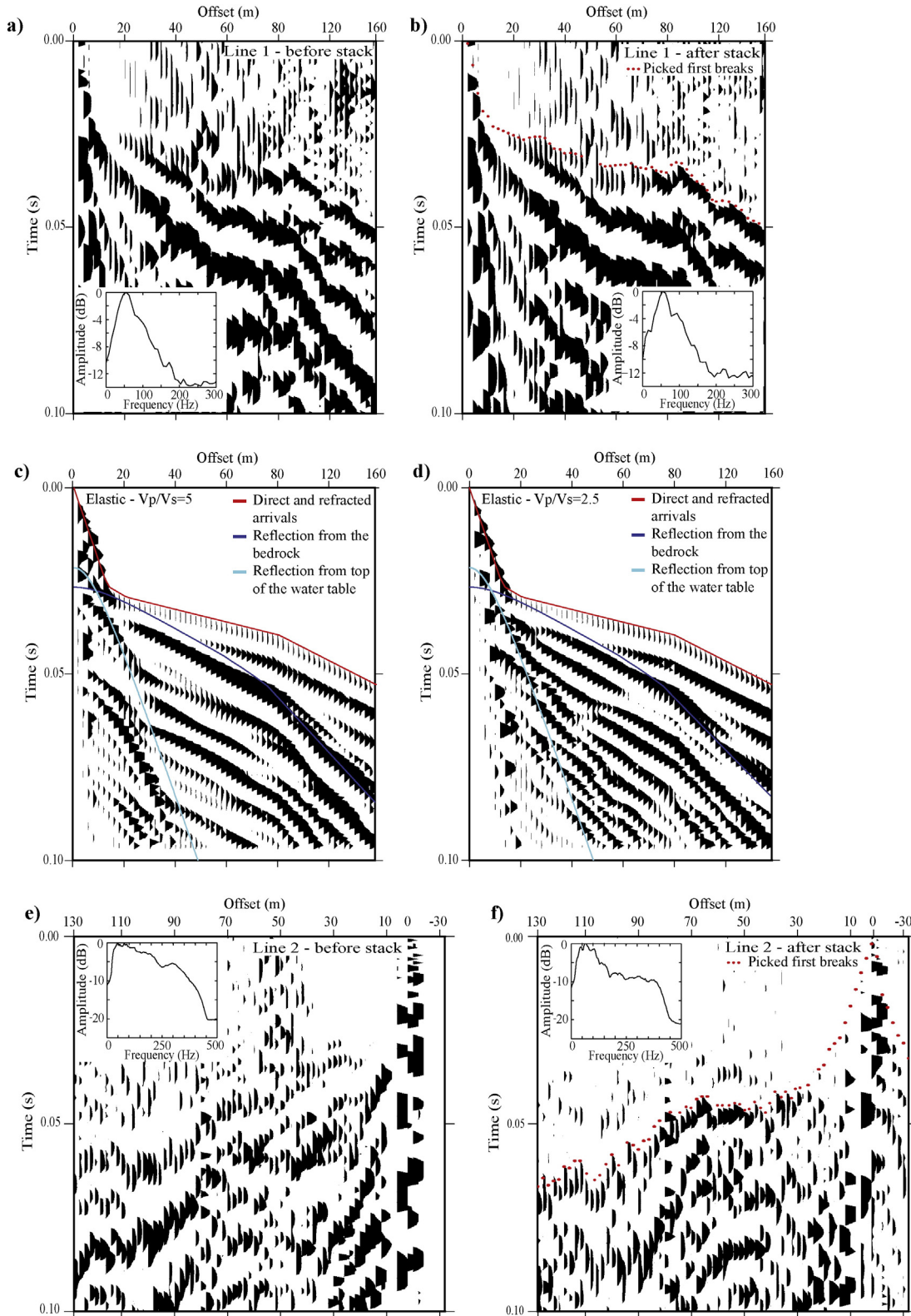


**Fig. 9.** Example shot gathers from the two seismic lines and their amplitude spectra from the Stockholm Bypass site. (a) Raw data (one hit) and (b) after vertical stacking of three repeated hits from Line 1 showing the quality of the data and first arrivals used for first arrival tomography. (c) Synthetic shot gather generated using an elastic finite-difference algorithm and a three layered earth model constrained from the actual seismic data using $V_P/V_S = 5$. Different color lines showing theoretical direct and refracted arrivals (red line), reflection from the top of water table (cyan, 5.5 m deep) and the bedrock (blue, ~12 m deep). (d) Synthetic shot gather with $V_P/V_S = 2.5$ and overlaid direct and refracted arrivals (red line), reflection from the top of water table (cyan, 5.5 m deep) and the bedrock (blue, ~12 m deep). (e) Raw data and (f) after vertical stacking of three repeated hits with first breaks overlaid from Line 2.

crookedness of the lines and topography variations. A good starting model was the key for obtaining a good velocity model from these lines. To generate the starting model, near offset traveltimes were used. To avoid rays channeling above the topography, the starting model had to be carefully constructed so that regions above it used velocities on the order of 340 m/s (air velocity) and slightly higher than that in the shallow subsurface. This was particularly important for the data along Line 2 given the rapid topography changes. Details of the tomography algorithm can be found in Tryggvason et al. (2002). The final tomographic models (Fig. 10) had an RMS of about 3 ms (after 7 iterations), which was assumed to be sufficient and geologically reasonable, given the noisy nature of some traces and the quality of the first breaks (Fig. 9). The tomography was done using a cell size of 2 m in both the horizontal and vertical directions. Clear shear wave arrivals on the horizontal component data were not present so no shear wave tomography or joint P- and S-wave tomography using the same code, was performed. Information from existing boreholes close to the seismic lines, drilled for a preliminary phase of site investigations, is plotted on the tomography models (Fig. 10). A good match can be seen between the boreholes, our field observations on the locations of the outcrops and the tomography results, with the deviations from the aforesaid corresponding to offsets between the seismic lines and borehole positions. Zones with poor quality rock are reasonably well delineated by low velocity zones, especially as marked in Fig. 8. A slight mismatch between the velocities where the lines cross can be explained as a 3D effect with the rays coming from the side of the line, given its wiggly character and large topographic variations.

To give an estimation of the quality of our picked first breaks, they are shown in Fig. 11a as a function of offset (Line 1 only). Fig. 11b shows traveltime residuals (picked times minus forward calculated times) as a function of offset for the iteration used to present the velocity model in this study. A good match between picked and calculated values with most of the data falling in the error range of 2 ms can be seen. It is interesting to observe clustering of the first breaks into two distinct domains (Fig. 11a). These two domains correspond to two different overburden thicknesses in different parts of the line. This is consistent with the tomography results suggesting a sudden rise of bedrock (high-velocity materials) about 300 m distance along Line 1 (Fig. 10a).

To further illustrate the value of the landstreamer for urban applications we obtained parts of the tunnel model (Stockholm Bypass), including the access ramp, and visualized it with the tomography results obtained in this test and the LiDAR data (Fig. 12). The 3D visualization clearly illustrates how the poor quality rock correlate with a relatively

low velocity zone (3000–4000 m/s) and a change in the bedrock geometry (interpreted from the tomography models; Fig. 10a) suggesting the possibility of a fracture system and a small depression zone in the middle of Line 2.

## 4. Discussion

The MEMS-based 3C landstreamer developed in this study was tested in various places and the results illustrate its capability for imaging and site characterizations, especially in noisy environments. The first backyard test (Fig. 3) indicates the importance of obtaining broadband data. Both MEMS-based 3C sensors mounted on the streamer and the 10 Hz planted geophones image a clear reflection that is notably missing in the 28 Hz planted geophones. The horizontal components of the MEMS-based sensors from the streamer also show evidences of a mode-converted reflection. This mode-converted reflection indicates that there is an imaging potential of the 3C landstreamer using mode converted waves (Eaton and Stewart, 1989; Guy, 2004; Stewart et al., 2002; Stotter and Angerer, 2011). The amplitude spectra of the landstreamer sensors show more energy in the higher frequency part of the signal compared with the geophones tested, making them more suitable for near surface applications (Fig. 3f, g).

The sleds carrying the sensors on the landstreamer do not induce any significant energy decrease, phase difference or additional mode conversions (Fig. 4). We can also observe that the sleds used to mount the units on the landstreamer do not introduce additional phase change or time delays in the data. Judging from the amplitude spectra shown on Fig. 4, it appears that the landstreamer mounted DSU3s are slightly less sensitive to higher frequencies compared with planted ones. This difference is most likely due to site conditions and difference in ground coupling and will be investigated in detail in the near future. The nearest offset traces on the horizontal crossline component occasionally show a tuning effect on some phases (merging two phases into one). This phase behavior could be due to local ground conditions or introduced by the sleds due to bad coupling between them and the surface and is an effect that will be studied more in the future. Amplitude spectra and particle motion plots further support the similar nature of the data for the planted and the streamer mounted MEMS-based sensors. A similar comparison, but using a shear wave source, might be better suited for these types of tests and will be conducted in the near future.

The test with the shear wave vibrator was instructive in the sense that it showed the effect of ground conditions for collecting shear wave data. In soft sediments or over some grassy fields it is unlikely
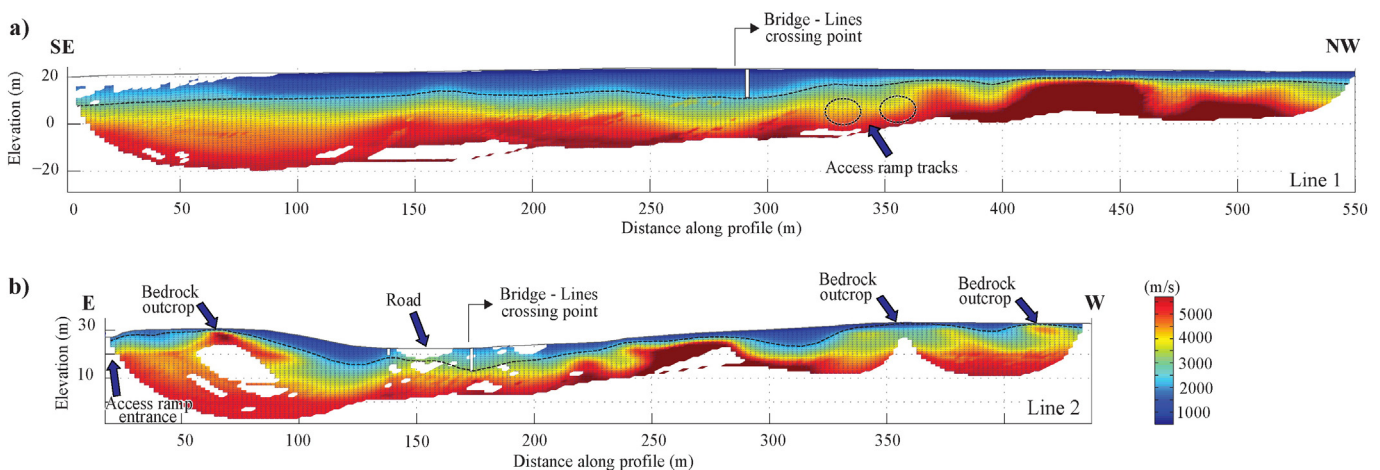


**Fig. 10.** 3D traveltime tomography results shown with the location of existing boreholes (white bars) identifying the bedrock level at (a) Line 1 and (b) Line 2. Results are shown along the receiver lines where the high-density ray coverage is present (note that the inversion was done in 3D). Arrows show major anthropogenic features, existing bedrock outcrops and approximate location of the access ramps and the black dashed line interpreted depth to the bedrock.
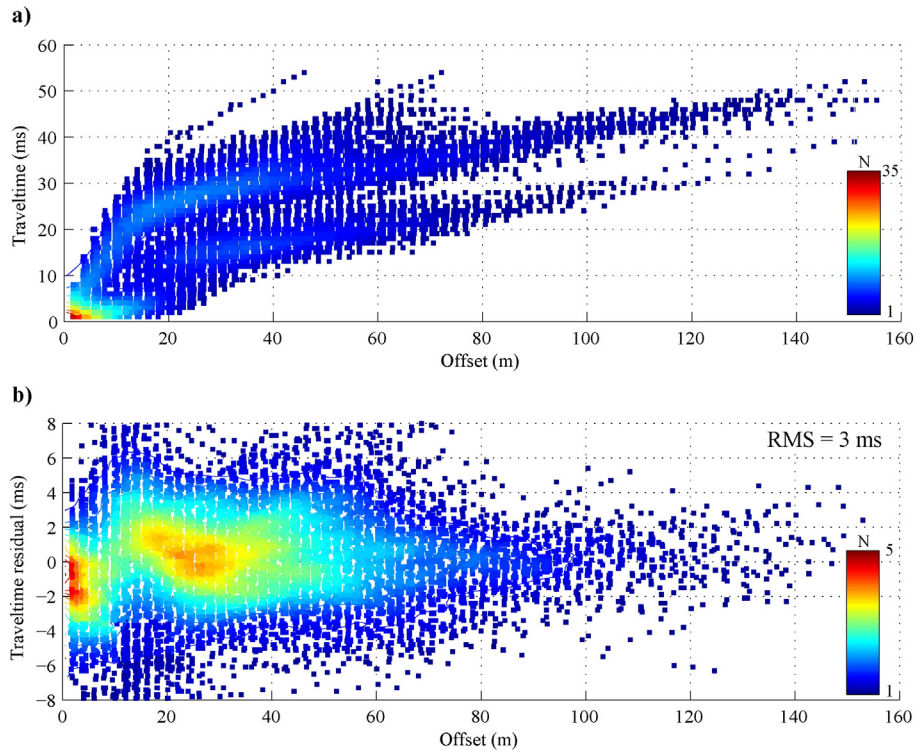
**Fig. 11.** Quality of the picked first arrivals and the inverted models. (a) Example of picked first breaks as a function of offset for Line 1. (b) Traveltime residuals versus offset for the same line after last iteration of the tomography inversion, with RMS value of 3 ms obtained. Colors correspond to number of points (N) within that range.
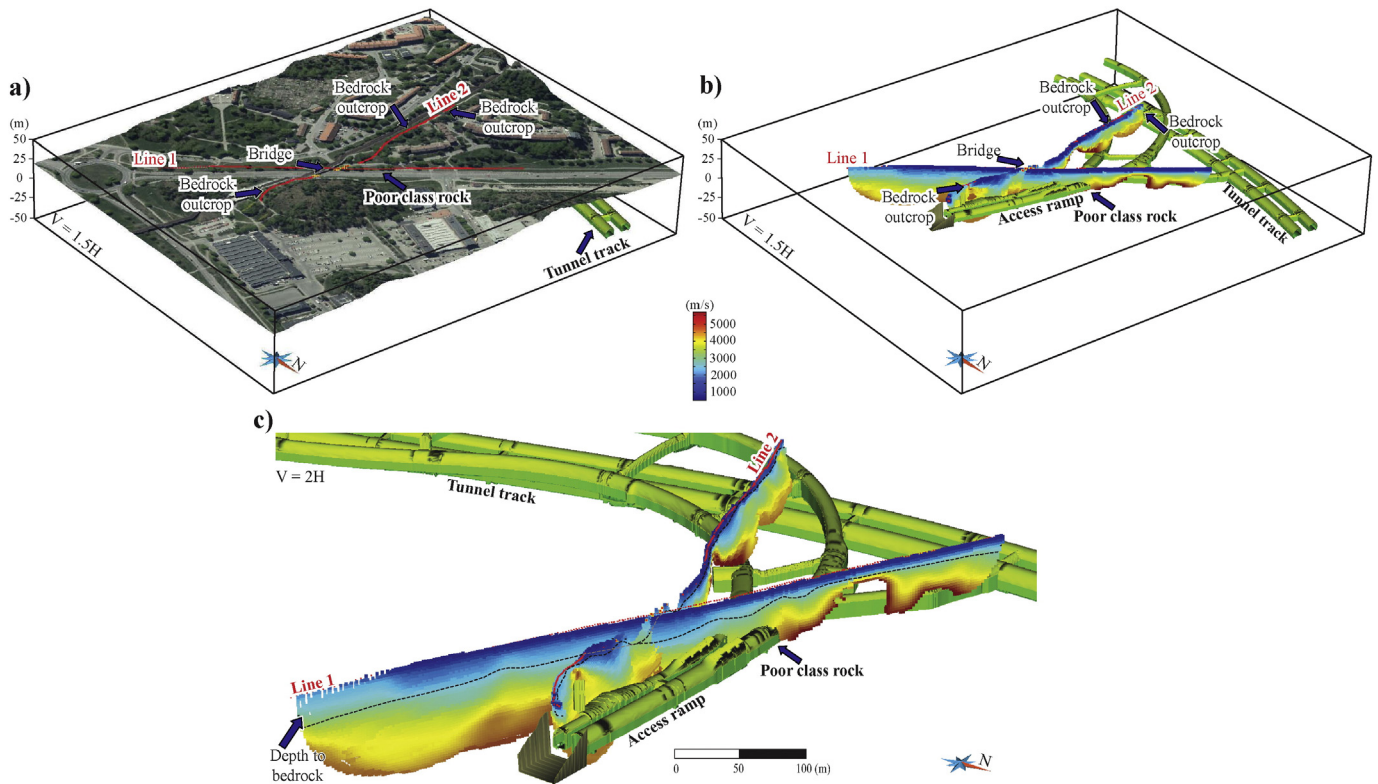


**Fig. 12.** 3D views showing visualization of the refraction tomography results with the model of the planned tunnel and the access ramp. (a) Aerial photo projected onto the elevation data obtained from LiDAR measurements showing the location of the seismic profiles and main anthropogenic features. (b) Tomography results (3D model) visualized with the tunnel indicating a low velocity zone where the bedrock deepens and where rocks have poor quality. (c) Closer view on the tomography results along with the interpreted depth to the bedrock (black dashed line) and the planned tunnel model. The tunnel model was kindly provided by the Swedish Transport Administration (Trafikverket).

that the use of high-frequency sweeps would be useful since the higher frequencies tend to attenuate quickly (Fig. 6). Even though the source frequencies were not adapted to the site requirements, judging from the shot gathers shown on Fig. 6b, c the high sensitivity of the landstreamer sensors might be the reason we were still able to identify the first arrivals. Comparing the gathers on Fig. 6a to b, c, we note that no contamination with mode leaked P waves is observed and how increasing the source sweep frequencies influences the data. We note from Fig. 6d that not much of the signal can be seen above 100 Hz, therefore better data might have been obtained using source sweeps with lower frequencies. A test conducted by Krawczyk et al. (2013); see also Malehmir et al., 2013a,b) on both a gravel road and farm field (mainly saturated clay) showed that imaging structures at that site using a seismic streamer is possible, but that the quality of the image is significantly different from the farm side than the gravel side. In fact, an issue to consider that favors the use of a multicomponent streamer, especially horizontal crossline data, is the possible absence of Love-waves from the experiments conducted over gravel roads, particularly if the materials below the compacted gravels have lower velocities than the surface. In this case, less Love-waves will be recorded or generated (Krawczyk et al., 2012, 2013; Polom et al., 2013). A thin layer of frozen ground (winter surveys) can also be suitable for such experiments using the streamer (e.g., Malehmir et al., 2015).

Given the urban characteristics of Stockholm Bypass, along with a significant amount of noise observed on the shot gathers, the streamer was still able to record fairly good quality data (Fig. 9). First breaks were picked relatively easily using an automatic picking algorithm. They were later inspected and manually modified (wherever needed), at least for Line 1. Picking first arrivals along Line 2 was more difficult due to bedrock outcrops and the fact that some of the sensors were actually situated on them (or occasionally on the stairs). This produced a level of uncertainty in the first breaks and required investing more time in the picking, compared to Line 1. Nevertheless, a matching result with the drilled boreholes and bedrock outcrops was obtained. Judging from the synthetic shot gathers (Fig. 9c, d), we argue that reflection seismic imaging of the bedrock is unlikely at this site and requires much denser station spacing between the sensors and sources with much higher frequency (Inazaki, 2006; Pugin et al., 2013a; Sloan et al., 2007). The streamer is built so that shorter spacing between the sensors can be achieved and this configuration will be tested in the future studies.

Tomography results along Line 1 (Fig. 10a) suggest that the bedrock deepens towards the southeastern side of the line, but with sharp changes in elevation where the poor quality rocks are observed. The sudden change in the bedrock topography may be an indication of fracturing or faulting, hence the poor quality of rocks at this location. Bedrock in the northwestern side of the line is as shallow as a couple of meters. This is also supported by the two clusters of the first breaks as shown in Fig. 11a. The tomography results along Line 2 (Fig. 10b) suggest an undulating bedrock surface with its deepest point where the road is located (Fig. 8). At almost every location where velocities more than 5000 m/s are observed near the surface there is bedrock outcropping (our observations), supporting the tomography results and further showing the potential of the streamer for this type of application.

At the Stockholm Bypass site we can also note the importance of the GPS time stamped wireless units merged with the streamer system that allowed the delineation of a depression zone that might pose a problem during tunnel construction. Judging from Fig. 12c, the access ramp will be located beneath this zone, where potentially lateral water flow might be expected. Recent information provided by the Swedish Transport Administration (Trafikverket) suggest that the materials above the planned access ramp tunnels (at least one of the two; Fig. 12c) at this location are so weak that a jet grouting program is planned to be conducted prior to their excavation/construction (Ulf B. Eriksson, personal communication, August 2015). This study thus further illustrates the

potential of the streamer and its combination with wireless sensors for complex field situations.

While the streamer and the data from it should be further analyzed and tested, we suggest it as a tool for urban applications. There are, however, limitations with the streamer and the data acquisition system used in conjunction with it. In its present configuration, a GPS signal is required. This is mainly for time stamping and data sampling since there is no internal clock in the acquisition system with the required accuracy. If a tunnel experiment is planned, the data recording system must be changed (not the streamer) or a GPS signal needs to be fed into the system, for example using an external clock generating a GPS protocol signal. We are currently working on developing an accurate (and synchronized with GPS) external clock that can locally transmit a GPS protocol signal to the acquisition system and wireless sensors. This is not needed if a surface experiment with the streamer is the goal.

Future studies should also aim at exploiting the potentials of the MEMS sensors for full waveform inversion in near surface environments, given their wider bandwidth, particularly at low frequencies. Towing the streamer segments in parallel might also be an option, and will be conducted in the future in the necessity of a high resolution shallow 3D reflection imaging surveys (e.g. Bachrach and Mukerji, 2001). Three component data and their ability to differentiate between Love- and Rayleigh-waves is another advantage to study (Boiero and Socco, 2014; Socco and Garofalo, 2012; Socco and Strobbia, 2004). These data are complementary and useful for near surface studies since most of these applications deal with the top few meters of the subsurface where there may not be any reflective structures or reflection imaging is difficult (Baker, 1999; Baker et al., 2000; Garotta, 1999; Steeples and Miller, 1998). In combination with the streamer, higher frequency sources should also be developed to take advantage of the broadband nature of the sensors. Future surveys will further explore the usefulness of the multi-component data acquisition. Until then, the current paper provides basic information about the streamer, its reliability and potential for near surface applications.

## 5. Conclusions

A three-component MEMS-based seismic landstreamer has been developed and tested against planted geophones and similar type sensors as used on the streamer. The broadband nature of the sensors, combined with insensitivity to electrical and electromagnetic noise, makes the system superior to its geophone-type predecessors, especially in urban environments. Tests conducted with the shear wave vibrator showed that a compacted (and saturated) ground is likely required to take the full advantages of the broadband nature of the sensors. Otherwise in dry and highly porous medium, it is unlikely that shear wave frequencies higher than 100 Hz are recorded at the medium to far offsets (50–200 m). As a complementary study, part of the planned Stockholm Bypass tunnel was chosen where depth to the bedrock and a potential weak zone were our main targets. A combination of the streamer with wireless recorders was used to perform 3D first arrival tomography. These results in combination with borehole information, and our own field observations, further demonstrated the capability of the system for urban site characterization. The potential reflection seismic imaging of the bedrock at the Stockholm Bypass site was evaluated through elastic finite-difference seismic modeling. The modeling showed the difficulty in imaging reflections from the bedrock at this site with the given acquisition parameters, but at the same time supported the initial model used to generate synthetic shot gathers when compared with real shot gathers. Although these initial studies of the system do not fully exploit the benefits of 3C MEMS-based sensors, no negative effect such as phase or time difference, polarity change or other effects induced by the overall landstreamer assembly have been noted. The results obtained with the streamer indicate a better signal quality compared to the geophones tested, while the sensitivity and

broadband nature of the 3C sensors open great potential to use it for various near surface applications.

## Acknowledgments

## References

Adamczyk, A.A., Malinowski, M., Malehmir, A., 2014. high-resolution near-surface velocity model building using full-waveform inversion — a case study from southwest Sweden. Geophys. J. Int. 197, 1693–1704. http://dx.doi.org/10.1093/gji/ggu070.

Alcudia, A.A., Stewart, R., Hall, K., Gallant, E., 2008. Field comparison of 3-C geophones and microphones to high-precision blasting sensors. CREWES Res. Rep. 20, 1–20.

Almholt, A.A., Wisén, R., Jorgensen, R., Ringgaard, J., Nielsen, U., 2013. High resolution 2D reflection seismic land streamer survey for groundwater mapping: Case study from southeast Denmark. SEG Technical Program Expanded Abstracts 2013. Society of Exploration Geophysicists, pp. 1894–1898.

Bachrach, R., Mukerji, T., 2001. Fast 3D ultra shallow seismic reflection imaging using portable geophone mount. Geophys. Res. Lett. 28, 45–48. http://dx.doi.org/10.1029/2000GL012020.

Bachrach, R., Nur, A.A., 1998. Ultra shallow seismic reflection in unconsolidated sediments: Rock physics base for data acquisition. SEG Tech. Program Expand. Abstr. 1998, pp. 866–869.

Baker, G., 1999. Processing near-surface seismic-reflection data. CCourse Notes Series. Society of Exploration Geophysicists.

Baker, G., Steeples, D., Schmeissner, C., Spikes, K., 2000. Collecting seismic-reflection data from depths shallower than three meters. Symposium on the Application of Geophysics to Engineering and Environmental Problems. Environment and Engineering Geophysical Society, pp. 1207–1214.

Bansal, R., Gaiser, J., 2012. An introduction to this special section: applications and challenges in shear-wave exploration. Lead. Edge 32, 12-12. http://dx.doi.org/10.1190/tle32010012.1.

Boiero, D., Socco, L.V., 2014. Joint inversion of Rayleigh-wave dispersion and P-wave refraction data for laterally varying layered models. Geophysics 79, EN49–EN59. http://dx.doi.org/10.1190/geo2013-0212.1.

Bretaudeau, F., Leparoux, D., Abraham, O., 2008. Small scale adaptation of the seismic full waveform inversion method — application to civil engineering applications. Acoust. 08 Paris.

Deidda, G.P., Ranieri, G., 2001. Some SH-wave seismic reflections from depths of less than three metres. Geophys. Prospect. 49, 499–508. http://dx.doi.org/10.1046/j.1365-2478.2001.00280.x.

Determann, J., Thyssen, F., Engelhardt, H., 1988. Ice thickness and sea depth derived from reflection-seismic measurements on the central part of Filchner-Ronne Ice Shelf, Antarctica. Ann. Glaciol. 11.

Eaton, D., Stewart, R., 1989. Aspects of seismic imaging using P-SV converted waves. CREWES Res. Rep. 6, 68–92.

Eiken, O., Degutsch, M., Riste, P., Rød, K., 1989. Snowstreamer: an efficient tool in seismic acquisition. First Break 7. http://dx.doi.org/10.3997/1365-2397.1989021.

Fabien-Ouellet, G., Fortier, R., 2014. Using all seismic arrivals in shallow seismic investigations. J. Appl. Geophys. 103, 31–42. http://dx.doi.org/10.1016/j.jappgeo.2013.12.009.

Garotta, R., 1999. Shear waves from acquisition to interpretation. Distinguished Instructor Series. Society of Exploration Geophysicists.

Gibson, J., Burnett, R., 2005. Another look at MEMS sensors… and dynamic range. CSEG Rec. 20.

Gibson, J., Burnett, R., Ronen, S., Watt, H., 2005. MEMS sensors: some issues for consideration. Lead. Edge 24, 786–790. http://dx.doi.org/10.1190/1.2032249.

Guy, E.D., 2004. Evaluation of near-surface converted-mode seismic reflection imaging potential. Electron. J. Geotech. Eng. 9, 1–35.

Hardage, B., DeAngelo, M., Murray, P., Sava, D., 2011. 3. Multicomponent Data processing. Multicomponent Seismic TechnologyGGeophysical References Series. Society of Exploration Geophysicists, pp. 77–124.

Hauer, G., Hons, M., Kendall, R., Lawton, D., Bertram, M., 2008. Field data comparison: 3C–2D data acquisition with geophones and accelerometers. SEG Technical Program Expanded Abstracts 2008. Society of Exploration Geophysicists, pp. 178–182.

Heijkenskjöld, R., 2001. Landskapsutveckling i Uppsalatrakten. Naturkonsulten, Uppsala.

Hons, M.S., 2008. Seismic sensing: comparison of geophones and accelerometers using laboratory and field data CREWES Theses 2008.

Hons, M., Stewart, R., Lawton, D., Bertram, M., 2007. Ground motion through geophones and MEMS accelerometers: sensor comparison in theory, modeling, and field data. SEG Technical Program Expanded Abstracts 2007. Society of Exploration Geophysicists, pp. 11–15.

Huggins, R., 2004. A report on land streamers: the last geophone you will ever plant? Surf. Views -Surf. Geophys. Sect. Soc. Explor. Geophys. SEG, first quarter vol. 11

Inazaki, T., 1999. Land Streamer; a new system for high-resolution S-wave shallow reflection surveys. Proc. 12th Annu. Symp. Appl. Geophys. Eng. Environ. Probl. SAGEEP1999, pp. 207–216.

Inazaki, T., 2004. High-resolution seismic reflection surveying at paved areas using an S-wave type Land Streamer. Explor. Geophys. 35. http://dx.doi.org/10.1071/EG04001.

Inazaki, T., 2006. High-resolution S-wave reflection survey in urban areas using a woven belt type Land streamer. Surf. 2006 Sept. 4-6 Hels. Finl.

Juhlin, C., 1995. Finite-difference elastic wave propagation in 2D heterogeneous transversely isotropic media. Geophys. Prospect. 43, 843–858. http://dx.doi.org/10.1111/j.1365-2478.1995.tb00284.x.

Juhlin, C., Sturkell, E., Ebbestad, J.O.R., Lehnert, O., Högström, A.E.S., Meinhold, G., 2012. A new interpretation of the sedimentary cover in the western Siljan Ring area, central Sweden, based on seismic data. Tectonophysics 580, 88–99. http://dx.doi.org/10.1016/j.tecto.2012.08.040.

Keho, T., Kelamis, P., 2009. A new era in land seismic: The near surface challenge. SEG Technical Program Expanded Abstracts 2009. Society of Exploration Geophysicists, pp. 3421–3425.

Kendall, R., 2006. Advances in land multicomponent Seismic: acquisition, processing and Interpretation. CSEG Rec. 31, 65–75 (doi: http://csegrecorder.com/editions/issue/2006-03).

Krawczyk, C., Polom, U., Trabs, S., Dahm, T., 2012. Sinkholes in the city of Hamburg — new urban shear-wave reflection seismic system enables high-resolution imaging of subrosion structures. J. Appl. Geophys. 78, 133–143. http://dx.doi.org/10.1016/j.jappgeo.2011.02.003.

Krawczyk, C., Polom, U., Beilecke, T., 2013. Shear-wave reflection seismics as a valuable tool for near-surface urban applications. Lead. Edge 32, 256–263. http://dx.doi.org/10.1190/tle32030256.1.

Kruppenbach, J.A., Bedenbender, J.W., 1975. United States Patent: 3923121 — Towed land cable. 3923121.

Lai, C.G., Rix, G.J., Foti, S., Roma, V., 2002. Simultaneous measurement and inversion of surface wave dispersion and attenuation curves. Soil Dyn. Earthq. Eng. 22, 923–930. http://dx.doi.org/10.1016/S0267-7261(02)00116-1.

Laine, J., Mougenot, D., 2014. A high-sensitivity MEMS-based accelerometer. Lead. Edge 33, 1234–1242. http://dx.doi.org/10.1190/tle33111234.1.

Lawton, D.C., Bertram, M.B., Margrave, G.F., Gallant, E.V., 2006a. Comparisons between data recorded by several 3-component coil geophones and a MEMS sensor at the Violet Grove monitor seismic survey. CREWES Res. Rep. 18, 1–24.

Link, C., Speece, M., Betterly, S., 2006. An Overview of Seismic Land Streamer Projects at Montana Tech. Presented at the Symposium on the Application of Geophysics to Engineering and Environmental Problems 2006. Environment and Engineering Geophysical Society, pp. 1012–1026.

Lundin, S.-E., 1988. Ingenjörsgeologisk Karta Över Uppsala: Engineering Geological map of City of Uppsala. Uppsala university, Uppsala 0348-2979 ; 154.

Malehmir, A., Bastani, M., Krawczyk, C., Gurk, M., Ismail, N., Polom, U., Persson, L., 2013a. Geophysical assessment and geotechnical investigation of quick-clay landslides —+ a Swedish case study. Surv. Geophys. 11. http://dx.doi.org/10.3997/1873-0604.2013010.

Malehmir, A., Saleem, M.U., Bastani, M., 2013b. High-resolution reflection seismic investigations of quick-clay and associated formations at a landslide scar in southwest Sweden. J. Appl. Geophys. 92, 84–102. http://dx.doi.org/10.1016/j.jappgeo.2013.02.013.

Malehmir, A., Wang, S., Lamminen, J., Brodic, B., Bastani, M., Vaittinen, K., Juhlin, C., Place, J., 2015. Delineating structures controlling sandstone-hosted base-metal deposits using high-resolution multicomponent seismic and radio-magnetotelluric methods: a case study from Northern Sweden. Geophys. Prospect. 63, 774–797. http://dx.doi.org/10.1111/1365-2478.12238.

Merchant, J., 2009. MEMS Applications in Seismology. Presented at the Seismic Instrumentation Technology Symposium, Palm Springs, CA (http://www.iris.edu/hq/instrumentation_meeting/files/pdfs/MEMS_Seismology.pdf).

Miller, R., Pullan, S., Waldner, J., Haeni, F., 1986. Field comparison of shallow seismic sources. Geophysics 51, 2067–2092. http://dx.doi.org/10.1190/1.1442061.

Mougenot, D., Thorburn, N., 2004. MEMS-based 3D accelerometers for land seismic acquisition: Is it time? Lead. Edge 23, 246–250. http://dx.doi.org/10.1190/1.1690897.

Mougenot, D., Cherepovskiy, A., JunJie, L., 2011. MEMS-based accelerometers: expectations and practical achievements. First Break 29.

Paasche, H., Rumpf, M., Hausmann, J., Fechner, T., Werban, U., Tronicke, J., Dietrich, P., 2013. Advances in acquisition and processing of near-surface seismic tomographic data for geotechnical site assessment. First Break 31.

Park, C., Miller, R., Xia, J., 1999. Multichannel analysis of surface waves. Geophysics 64, 800–808. http://dx.doi.org/10.1190/1.1444590.

Park, C.B., Miller, R.D., Miura, H., 2002. Optimum field parameters of an MASW survey [Exp. Abs.]. SEG-J, Tokyo, pp. 22–23.

Place, J., Malehmir, A., Högdahl, K., Juhlin, C., Persson Nilsson, K., 2015. Seismic characterization of the Grängesberg iron deposit and its mining-induced structures, central Sweden. Interpretation (in print).

Polom, U., Druivenga, G., Grossmann, E., Grüneberg, S., Rode, W., 2011. Transportabler Scherwellenvibrator: Deutsches Patent und Markenamt. Patentschrift DE10327757B4.

Polom, U., Bagge, M., Wadas, S., Winsemann, J., Brandes, C., Binot, F., Krawczyk, C.M., 2013. Surveying near-surface depocentres by means of shear wave seismics. First Break 31.

Pugin, A.J.M., Larson, T., Bergler, S., McBride, J., Bexfield, C., 2004a. Near-surface mapping using SH-wave and P-wave seismic land-streamer data acquisition in Illinois, U.S. Lead. Edge 23, 677–682. http://dx.doi.org/10.1190/1.1776740.

Pugin, A.J.M., Larson, T., Sargent, S., 2004b. 3.5 km/day of high resolution seismic reflection data using a landstreamer. Presented at the Symposium on the Application of Geophysics to Engineering and Environmental Problems 2004. Environment and Engineering Geophysical Society, pp. 1380–1388.

Pugin, A.J.M., Pullan, S., Hunter, J., Oldenborger, G., 2009. Hydrogeological prospecting using P- and S-wave landstreamer seismic reflection methods. Surv. Geophys. 7. http://dx.doi.org/10.3997/1873-0604.2009033.

Pugin, A.J.M., Pullan, S., Duchesne, M., 2013a. Regional hydrostratigraphy and insights into fluid flow through a clay aquitard from shallow seismic reflection data. Lead. Edge 32, 742–748. http://dx.doi.org/10.1190/tle32070742.1.

Pugin, A.J.M., Pullan, S., Hunter, J.A., 2013b. Shear-wave high-resolution seismic reflection in Ottawa and Quebec City, Canada. Lead. Edge 32, 250–255. http://dx.doi.org/10.1190/tle32030250.1.

Pullan, S., Pugin, A., Hunter, J., Cartwright, T., Douma, M., 2008. Application of P-wave seismic reflection methods using the Landstreamer/Minivib system to near-surface investigations. Presented at the Symposium on the Application of Geophysics to Engineering and Environmental Problems 2008. Environment and Engineering Geophysical Society, pp. 614–625.

Sirgue, L., Barkved, O.I., Dellinger, J., Etgen, J., Albertin, U., Kommedal, J.H., 2010. Thematic set: full waveform inversion: the next leap forward in imaging at Valhall. First Break 28. http://dx.doi.org/10.3997/1365-2397.2010012.

Sloan, S.D., Tsoflias, G.P., Steeples, D.W., Vincent, P.D., 2007. High-resolution ultra-shallow subsurface imaging by integrating near-surface seismic reflection and ground-penetrating radar data in the depth domain. J. Appl. Geophys. 62, 281–286. http://dx.doi.org/10.1016/j.jappgeo.2007.01.001.

Socco, L.V., Garofalo, F., 2012. Joint inversion of surface wave and body wave data for the characterisation of a fault system in New Zealand. Presented at the EGU Gen. Assem. 2012, p. 1889.

Socco, L.V., Strobbia, C., 2004. Surface-wave method for near-surface characterization: a tutorial. Surv. Geophys. 2. http://dx.doi.org/10.3997/1873-0604.2004015.

Socco, L.V., Boiero, D., Foti, S., Wisén, R., 2009. Laterally constrained inversion of ground roll from seismic reflection records. Geophysics 74, G35–G45. http://dx.doi.org/10.1190/1.3223636.

Socco, L., Foti, S., Boiero, D., 2010. Surface-wave analysis for building near-surface velocity models — established approaches and new perspectives. Geophysics 75. http://dx.doi.org/10.1190/1.3479491 (75A83–75A102).

Sopher, D., Juhlin, C., Huang, F., Ivandic, M., Lueth, S., 2014. Quantitative assessment of seismic source performance: Feasibility of small and affordable seismic sources for long term monitoring at the Ketzin $CO_2$ storage site, Germany. J. Appl. Geophys. 107, 171–186. http://dx.doi.org/10.1016/j.jappgeo.2014.05.016.

Steeples, D.W., 2004. Near-surface seismic reflection applications. Presented at the 1st International Conference on Environmental and Engineering Geophysics, Wuhan, China.

Steeples, D., Miller, R., 1998. Avoiding pitfalls in shallow seismic reflection surveys. Geophysics 63, 1213–1224. http://dx.doi.org/10.1190/1.1444422.

Stewart, R., Gaiser, J., Brown, R., Lawton, D., 2002. Converted-wave seismic exploration: methods. Geophysics 67, 1348–1363. http://dx.doi.org/10.1190/1.1512781.

Stotter, C., Angerer, E., 2011. Evaluation of 3C microelectromechanical system data on a 2D line: Direct comparison with conventional vertical-component geophone arrays and PS-wave analysis. Geophysics 76, B79–B87. http://dx.doi.org/10.1190/1.3561769.

Suarez, G.M., Stewart, R.R., 2007. Acquisition and analysis of 3C land streamer data. CREWES Res. Rep. 19, 1–12 (doi:http://www.crewes.org/ForOurSponsors/ResearchReports/2007/2007-19.pdf).

Suarez, G.M., Stewart, R.R., 2008a. Side-by-side comparison of 3-C land streamer versus planted geophone data at the Priddis test site. CREWES Res. Rep. 20, 1–16.

Suarez, G.M., Stewart, R.R., 2008b. A field comparison of 3-C land streamer versus planted geophone data. SEG Technical Program Expanded Abstracts 2008. Society of Exploration Geophysicists, pp. 16–20.

Tryggvason, A., Bergman, B., 2006. A traveltime reciprocity discrepancy in the Podvin & Lecomte time 3d finite difference algorithm. Geophys. J. Int. 165, 432–435. http://dx.doi.org/10.1111/j.1365-246X.2006.02925.x.

Tryggvason, A., Rögnvaldsson, S., ður, T., Flóvenz, Ó.G., 2002. Three-dimensional imaging of the P- and S-wave velocity structure and earthquake locations beneath Southwest Iceland. Geophys. J. Int. 151, 848–866. http://dx.doi.org/10.1046/j.1365-246X.2002.01812.x.

van der Veen, M., Green, A.G., 1998. Land streamer for shallow seismic data acquisition; evaluation of gimbaled-mounted geophones. Geophysics 63, 1408–1413. http://dx.doi.org/10.1190/1.1444442.

van der Veen, M., Buness, H.A., Büker, F., Green, A.G., 2000. Field comparison of high-frequency seismic sources for imaging shallow (10–250 m) structures. J. Environ. Eng. Geophys. 5, 39–56.

van der Veen, M., Spitzer, R., Green, A., Wild, P., 2001. Design and application of a towed land-streamer system for cost-effective 2-D and pseudo-3-D shallow seismic data acquisition. Geophysics 66, 482–500. http://dx.doi.org/10.1190/1.1444939.

Xia, J., Miller, R.D., Park, C.B., Tian, G., 2003. Inversion of high frequency surface waves with fundamental and higher modes. J. Appl. Geophys. 52, 45–57. http://dx.doi.org/10.1016/S0926-9851(02)00239-2.

Zhang, F., Juhlin, C., Ivandic, M., Lüth, S., 2013. Application of seismic full waveform inversion to monitor $CO_2$ injection: modelling and a real data example from the Ketzin site, Germany. Geophys. Prospect. 61, 284–299. http://dx.doi.org/10.1111/1365-2478.12021.